Draft version November 2, 2012
Preprint typeset using LaTeX style emulateapj v. 8/13/10

arXiv:1211.0014v1 [astro-ph.CO] 31 Oct 2012

COLD ACCRETION IN EARLY GALAXY FORMATION AND ITS Lyα SIGNATURES

Hidenobu Yajima[1,2], Yuexing Li[1,2], Qirong Zhu[1,2], Tom Abel[3]
[1]Department of Astronomy & Astrophysics, The Pennsylvania State University, 525 Davey Lab, University Park, PA 16802, USA
[2]Institute for Gravitation and the Cosmos, The Pennsylvania State University, University Park, PA 16802, USA and
[3]Kavli Institute for Particle Astrophysics and Cosmology, SLAC National Accelerator Laboratory, Stanford University,
2575 Sand Hill Road, Menlo Park, CA 94025, USA

Draft version November 2, 2012

ABSTRACT

The Lyα emission has played an important role in detecting high-redshift galaxies, including currently the most distant one at redshift $z = 8.6$. It may also contain important information on the origin of these galaxies. Here, we investigate the formation of a typical L^* galaxy and its observational signatures at the earliest stage, by combining a cosmological hydrodynamic simulation with three-dimensional radiative transfer calculations using the newly improved ART^2 code. Our cosmological simulation uses the Aquila initial condition which zooms in onto a Milky Way-like halo with high resolutions, and our radiative transfer couples multi-wavelength continuum, Lyα line, and ionization of hydrogen. We find that the modeled galaxy starts to form at redshift $z \sim 24$ through efficient accretion of cold gas, which produces a strong Lyα line with a luminosity of $L_{\mathrm{Ly}\alpha} \sim 10^{42}$ erg s^{-1} as early as $z \sim 14$. The Lyα emission appears to trace the cold, dense gas. The lines exhibit asymmetric, single-peak profiles, and are shifted to the blue wing, a characteristic feature of gas inflow. Moreover, the contribution to the total Lyα luminosity by excitation cooling increases with redshift, and it becomes dominant at $z \gtrsim 6$. We predict that L^* galaxies such as the modeled one may be detected at $z \lesssim 8$ by JWST and ALMA with a reasonable integration time. Beyond redshift 12, however, only Lyα line may be observable by narrow band surveys. Our results suggest that Lyα line is one of the most powerful tools to detect the first generation of galaxies, and to decipher their formation mechanism.

Subject headings: galaxies: formation – galaxies: evolution – galaxies: high-redshift – radiative transfer – line: profiles – hydrodynamics – cosmology: computation

1. INTRODUCTION

The quest for the first galaxies formed at the cosmic dawn is a major frontier in both observational and theoretical cosmology (Bromm & Yoshida 2011). Over the past few years, significant progress has been made in detecting galaxies at redshift $z \gtrsim 6$, using either broad-band colors (e.g., Bouwens et al. 2004; Bouwens & Illingworth 2006; Bouwens et al. 2010, 2011), or narrow-band Lyα emission line (e.g., Malhotra & Rhoads 2004; Iye et al. 2006; Stark et al. 2007; Hu et al. 2010; Lehnert et al. 2010; Vanzella et al. 2011; Stark et al. 2011; Ono et al. 2012; Kashikawa et al. 2011; Shibuya et al. 2012). In particular, the Lyα line has played an important role in identifying and confirming distant galaxies, the so-called Lyα emitters (LAEs), including currently the record holder at $z = 8.6$ (Lehnert et al. 2010). These remarkable observations indicate that galaxies formed less than a few hundred million years after the Big Bang.

Despite the rapidly increasing number of detections, the origin and nature of these distant galaxies, however, remain open questions (Bromm et al. 2009). Recently, a number of state-of-the-art simulations have started to address this issue (e.g., Wise & Abel 2007; Wise et al. 2008; Wise & Abel 2008; Greif et al. 2010; Wise et al. 2012; Jeon et al. 2012). These studies focused on a halo in a small volume (1 Mpc) with high resolutions, and suggested that the formation of the first galaxies is closely tied to the formation of the first stars (so-called Pop III stars) and the feedback from them, and that these galaxies likely consist of second- or third generation of stars formed from enriched gas, similar to the present-day stars.

In this work, we explore the physical conditions of early galaxy formation on a larger scale. In particular, we focus on the gas properties and the Lyα emission from it. Recent simulations have revealed that a large amount of gas penetrate deep inside dark matter halos as cold, filamentary streams (Katz et al. 2003; Birnboim & Dekel 2003; Kereš et al. 2005, 2009; Dekel & Birnboim 2006; Ocvirk et al. 2008; Brooks et al. 2009; Dekel et al. 2009), and Dekel et al. (2009) showed that massive galaxies at $z = 2 - 3$ can actively form stars from inflow of cold gas. More recently, Di Matteo et al. (2011) suggested that massive galaxies at $z \gtrsim 6$ can grow by cold accretion and evolve with black holes. Such streams of cold gas may produce a large number of Lyα photons via excitation cooling process, and give rise to the Lyα emission detected in the early galaxies (Dijkstra & Loeb 2009; Faucher-Giguère et al. 2010; Latif et al. 2011; Yajima et al. 2012a,b).

We combine a multi-scale cosmological hydrodynamic simulation with multi-wavelength radiative transfer (RT) calculations. The simulation uses the Aquila initial condition and follows the formation and evolution of a Milky Way-size galaxy (Wadepuhl & Springel 2011; Scannapieco et al. 2012). It covers a large dynamical range from a 100 h^{-1}Mpc box down to a ~ 5 h^{-3}Mpc

yuh19@psu.edu

zoom-in region, which is ideal to study the gas inflow on a large scale. The RT calculations uses the newly improved code ART^2 by Yajima et al. (2012a). The ART^2 code couples multi-wavelength continuum, Lyα line, and ionization of hydrogen, which is critical to study the Lyα and multi-band properties of the early galaxies.

The paper is organized as follows. We describe our cosmological simulation in §2, and the RT calculations in §3. In §4, we present the results, which include the Lyα properties, and detectability by upcoming missions *James Webb Space Telescope* (JWST) and *Atacama Large Millimeter Array* (ALMA). We discuss the implications and limitations of our model in §5, and summarize in §6.

2. GALAXY MODEL

The cosmological simulation presented here follows the formation and evolution of a Milky Way-like galaxy and its substructures. The simulation is described in detail in (Zhu et al. in prep.), and it has been employed in a series of RT calculations by Yajima et al. (2012a) and Yajima et al. (2012b). Here we briefly highlight some important features of the simulation.

It uses the Aquila initial condition, which is the hydrodynamical version (Wadepuhl & Springel 2011) of the initial condition of the Aquarius Project, the largest ever particle simulation of a Milky Way-sized dark matter halo (Springel et al. 2008). The simulation includes dark matter, gasdynamics, star formation, black hole growth, and feedback processes, and is performed using the parallel, N-body/Smoothed Particle Hydrodynamics (SPH) code GADGET-3, which is an improved version of that described in Springel et al. (2001); Springel (2005). GADGET implements the entropy-conserving formulation of SPH (Springel & Hernquist 2002) with adaptive particle smoothing, as in Hernquist & Katz (1989). Radiative cooling and heating processes are calculated assuming collisional ionization equilibrium (Katz et al. 1996; Davé et al. 1999). Star formation is modeled in a multi-phase ISM, with a rate that follows the Schmidt-Kennicutt Law (Schmidt 1959; Kennicutt 1998). Feedback from supernovae is captured through a multi-phase model of the ISM by an effective equation of state for star-forming gas (Springel & Hernquist 2003). The UV background model of Haardt & Madau (1996) is used.

We also include a model of galactic wind driven by stellar feedback, as introduced by Springel & Hernquist (2003). Similar to Wadepuhl & Springel (2011), we adopt a constant wind velocity of $v_{\rm wind} = 484$ km s^{-1}, a mass-loss rate that is twice of the star formation rate, and an energy efficiency of unity such that the wind carries 100% of the supernova energy. The wind direction is anisotropical, preferentially perpendicular to the galactic disk. This wind model causes an outflow of gas, transporting energy, matter and metals out of the galactic disk in proportion to the star formation rate (Springel & Hernquist 2003). Our model galaxy shows similar SFR, mass of halo, gas and stars with those of the G3 runs in Scannapieco et al. (2012).

The whole simulation falls in a periodic box of 100 h^{-1}Mpc on each side with a zoom-in region of a size $5 \times 5 \times 5$ h^{-3}Mpc^3. The spatial resolution is ~ 250 h^{-1} pc in the zoom-in region. The mass resolution of this zoom-in region is 1.8×10^6 $h^{-1}M_\odot$ for dark matter particles, 3×10^5 $h^{-1}M_\odot$ for gas, and 1.5×10^5 $h^{-1}M_\odot$ for star particles. The cosmological parameters used in the simulation are $\Omega_m = 0.25$, $\Omega_\Lambda = 0.75$, $\sigma_8 = 0.9$ and $h = 0.73$, consistent with the five-year results of the WMAP (Komatsu et al. 2009). The simulation evolves from $z = 127$ to $z = 0$.

In the simulation, a galaxy is identified as a group using the on-fly friends-of-friends (FOF) group finding algorithms, which links all baryon particles to their nearest dark matter neighbor with a dark matter linking length less than 20% of their mean spacing.

This simulation covers a large dynamical range with decent resolutions. It is deal to study the formation of the first generation of galaxies and their environments, in particular the gas accretion from a large scale. In this work, we focus on the most massive galaxy from six snapshots at redshift $z \sim 6 - 14$, representing a Milky Way-like galaxy in its infancy.

3. RADIATIVE TRANSFER

The RT calculations are performed using the 3D Monte Carlo RT code, All-wavelength Radiative Transfer with Adaptive Refinement Tree (ART^2), as recently developed by Yajima et al. (2012a). ART^2 was improved over the original version of Li et al. (2008), and features three essential modules: continuum emission from X-ray to radio, Lyα emission from both recombination and collisional excitation, and ionization of neutral hydrogen. The coupling of these three modules, together with an adaptive refinement grid, enables a self-consistent and accurate calculation of the Lyα properties, which depend strongly on the UV continuum, ionization structure, and dust content of the object. Moreover, it efficiently produces multi-wavelength properties, such as the spectral energy distribution and images, for direct comparison with multi-band observations. The detailed implementations of the ART^2 code are described in Li et al. (2008) and Yajima et al. (2012a). Here we focus on the Lyα calculations and briefly outline the process.

The Lyα emission is generated by two major mechanisms: recombination of ionizing photons and collisional excitation of hydrogen gas. In the recombination process, we consider ionization of neutral hydrogen by ionizing radiation from stars, active galactic nucleus (AGN), and UV background (UVB), as well as by collisions by high-temperature gas. The ionized hydrogen atoms then recombine and create Lyα photons via the state transition 2P → 1S. The Lyα emissivity from the recombination is

$$\epsilon_\alpha^{\rm rec} = f_\alpha \alpha_{\rm B} h\nu_\alpha n_{\rm e} n_{\rm HII}, \tag{1}$$

where $\alpha_{\rm B}$ is the case B recombination coefficient, and f_α is the average number of Lyα photons produced per case B recombination. Here we use $\alpha_{\rm B}$ derived in Hui & Gnedin (1997). Since the temperature dependence of f_α is not strong, $f_\alpha = 0.68$ is assumed everywhere (Osterbrock & Ferland 2006). The product $h\nu_\alpha$ is the energy of a Lyα photon, 10.2 eV.

In the process of collisional excitation, high temperature electrons can excite the quantum state of hydrogen gas by the collision. Due to the large Einstein A coefficient, the hydrogen gas can quickly occur de-excitation with the Lyα emission. The Lyα emissivity by the collisional excitation is estimated by

$$\epsilon_\alpha^{\rm coll} = C_{{\rm Ly}\alpha} n_{\rm e} n_{\rm HI}, \tag{2}$$

where $C_{\mathrm{Ly}\alpha}$ is the collisional excitation coefficient, $C_{\mathrm{Ly}\alpha} = 3.7 \times 10^{-17} \exp(-h\nu_\alpha/kT) T^{-1/2}$ ergs s^{-1} cm^3 (Osterbrock & Ferland 2006).

Once the ionization structure have been determined, we estimate the intrinsic Lyα emissivity in each cell by the sum of above Lyα emissivity, $\epsilon_\alpha = \epsilon_\alpha^{\mathrm{rec}} + \epsilon_\alpha^{\mathrm{coll}}$.

In RT calculations, dust extinction from the ISM is included. The dust content is estimated according to the gas content and metallicity in each cell, which are taken from the hydrodynamic simulation. The dust-to-gas ratio of the MW is used where the metallicity is of Solar abundance, and it is linearly interpolated for other metallicity. We use the stellar population synthesis model of GALAXEV (Bruzual & Charlot 2003) to produce intrinsic spectral energy distributions (SEDs) of stars for a grid of metallicity and age, and we use a simple, broken power law for the AGN (Li et al. 2008). A Salpeter (1955) initial mass function is used in our calculations.

In this work, we apply ART^2 to the selected galaxies from the cosmological simulation. In our post-processing procedure, we first calculate the RT of ionizing photons ($\lambda \leq 912$ Å) and estimate the ionization fraction of the ISM. The resulting ionization structure is then used to run the Lyα RT to derive the emissivity, followed by the calculation of non-ionizing continuum photons ($\lambda > 912$ Å) in each cell. Our fiducial run is done with $N_{\mathrm{ph}} = 10^5$ photon packets for each ionizing, Lyα, and non-ionizing components, which was demonstrated to show good convergence (Yajima et al. 2012a,b). The highest refinement of the adaptive grid corresponds to a cell size comparable to the spatial resolution of 250 pc in comoving coordinate of the hydrodynamic simulation.

4. RESULTS

The formation history of a Milky Way-like galaxy, its multi-band properties, and its connection to high-redshift Lyα emitters, have been presented in a series of papers (Zhu et al. in prep., Yajima et al. 2012a,b,c). Here we focus on the galaxy formation at its earliest evolutionary stage and the Lyα properties from $z \sim 6 - 14$.

4.1. *The Accretion of Cold Gas*

The modeled MW galaxy starts to form at $z \sim 24$. Figure 1 shows the distribution of gas density, gas temperature, and stellar density of the MW main progenitor from redshift $z \sim 14$ to $z \sim 6$. The gas follows the distribution of dark matter and exhibits filamentary structures. At $z \gtrsim 6$, the gas is predominantly cold, with a mean temperature of $\sim 10^4$ K. Stars form out of such cold gas, so they also distribute along the filaments.

The star formation at $z \gtrsim 6$ is fueled by efficient accretion of cold gas, as demonstrated in Figure 2. The gas accretion rate is defined as the inflow rate of gas within the virial radius of the modeled galaxy. It peaks around 10^4 K in all cases. At a later time, feedback from both stars and accreting BHs heats up the gas. Also, the gas can be heated by gravitational shocks during the infall. Therefore the accretion includes hot gas as well. The inflow gas falls along the filaments toward the intersection, the highest density peak where the first galaxy in the simulated volume forms.

Figure 3 shows the star formation history of the MW. The star formation rate (SFR) increases steadily from $\sim 3 \times 10^{-3}$ M$_\odot$ yr^{-1} at $z \sim 24$ to ~ 15 M$_\odot$ yr^{-1} at $z \sim 8.5$, and it peaks at ~ 62 M$_\odot$ yr^{-1} at $z = 5.2$, owing to a merger of gas-rich protogalaxies. The galaxy mass increases rapidly during this cold accretion phase. By $z \sim 8.5$, it reaches a total mass of $\sim 5.6 \times 10^{10} M_\odot$, and a stellar mass of $\sim 6 \times 10^9 M_\odot$.

4.2. *The* Lyα *Properties*

The Lyα emission traces the gas distribution, as shown in Figure 4. The surface brightness rises above 10^{-20} ergs s^{-1} cm^{-2} arcsec^{-2} at $z \lesssim 14$. At high redshift $z \gtrsim 10$, the galaxy is small, and the Lyα emission is faint and confined to the central high-density region. As the galaxy grows in mass and size, the Lyα emission becomes stronger and more extended and irregular due to mergers and gas infall along the filaments of the main halo.

Figure 5 shows the Lyα properties of the MW galaxy at from $z \sim 14$ to $z \sim 6$, including the emergent Lyα luminosity ($L_{\mathrm{Ly}\alpha}$), equivalent width of Lyα line in rest frame, and photon escape fraction of Lyα and UV continuum (1300 - 1600 Å). For comparison with the star formation activity, the SFR of the galaxy at corresponding redshift is also shown.

During this early growth phase, the SFR of the galaxy increases from ~ 1 M$_\odot$ yr^{-1} at $z \sim 14.0$ to ~ 31 M$_\odot$ yr^{-1} at $z \sim 6$, owing to abundant supply of cold gas from infall and merging of gas-rich mini halos. The resulting emergent Lyα luminosity shows a similar trend, increasing from $\sim 1.6 \times 10^{42}$ erg s^{-1} at $z \sim 14.0$ to $\sim 5.5 \times 10^{42}$ erg s^{-1} at $z \sim 6$. If we consider only the recombination process with the assumption of $L_{\mathrm{Ly}\alpha}/L_{\mathrm{H}_\alpha} = 8.7$ (in which the H$_\alpha$ is a tracer of star formation), the the intrinsic Lyα luminosity should be linearly proportional to SFR, $L_{\mathrm{Ly}\alpha}$ (erg s^{-1}) $= 1.1 \times 10^{42} \times SFR$ (M$_\odot$ yr^{-1}) (Kennicutt 1998). However, the evolution of $L_{\mathrm{Ly}\alpha}$ in Figure 5 differs from the SFR history. This is due to the contribution from excitation cooling to the Lyα emission as we will discuss later, and dust absorption of the Lyα photons. In particular, at $z \gtrsim 10$, the $L_{\mathrm{Ly}\alpha}$ increases with redshift, in opposite direction from the SFR, as a result of high collisional excitation and high f_{esc}.

The lower-left panel of Figure 5 shows the photon escape fraction of Lyα, $f_{\mathrm{esc}}^{\mathrm{Ly}\alpha}$, and the UV continuum $f_{\mathrm{esc}}^{\mathrm{UV}}$, where $f_{\mathrm{esc}}^{\mathrm{UV}}$ is calculated at $\lambda_{\mathrm{rest}} = 1300 - 1600$ Å. The $f_{\mathrm{esc}}^{\mathrm{Ly}\alpha}$ of the modeled galaxy falls in the range of $0.49 - 0.81$, and it increases with redshift. In our model, the dust is produced by type-II supernovae (Li et al. 2008). The dust amount increases as star formation rises from $z \sim 14$ to $z \sim 6$, and hence it efficiently absorbs the Lyα and UV continuum photons, resulting decreasing escape fraction. However even at $z = 8.5$, about 40% of Lyα photons are absorbed by dust. This is due to the fact that, in the early phase, galaxies are gas rich and compact, the gas and dust are highly concentrated in the galaxies, resulting in effective absorption of the the Lyα and UV photons by the dust.

The resulting Lyα equivalent width (EW) is shown in the lower-right panel of Figure 5. The EW is defined by the ratio between the Lyα flux and the UV flux density f_{UV} in rest frame, where the mean flux density of $\lambda = 1300 - 1600$ Å is used. The modeled galaxy has EW $\gtrsim 20$ Å at these redshifts, and is therefore classi-

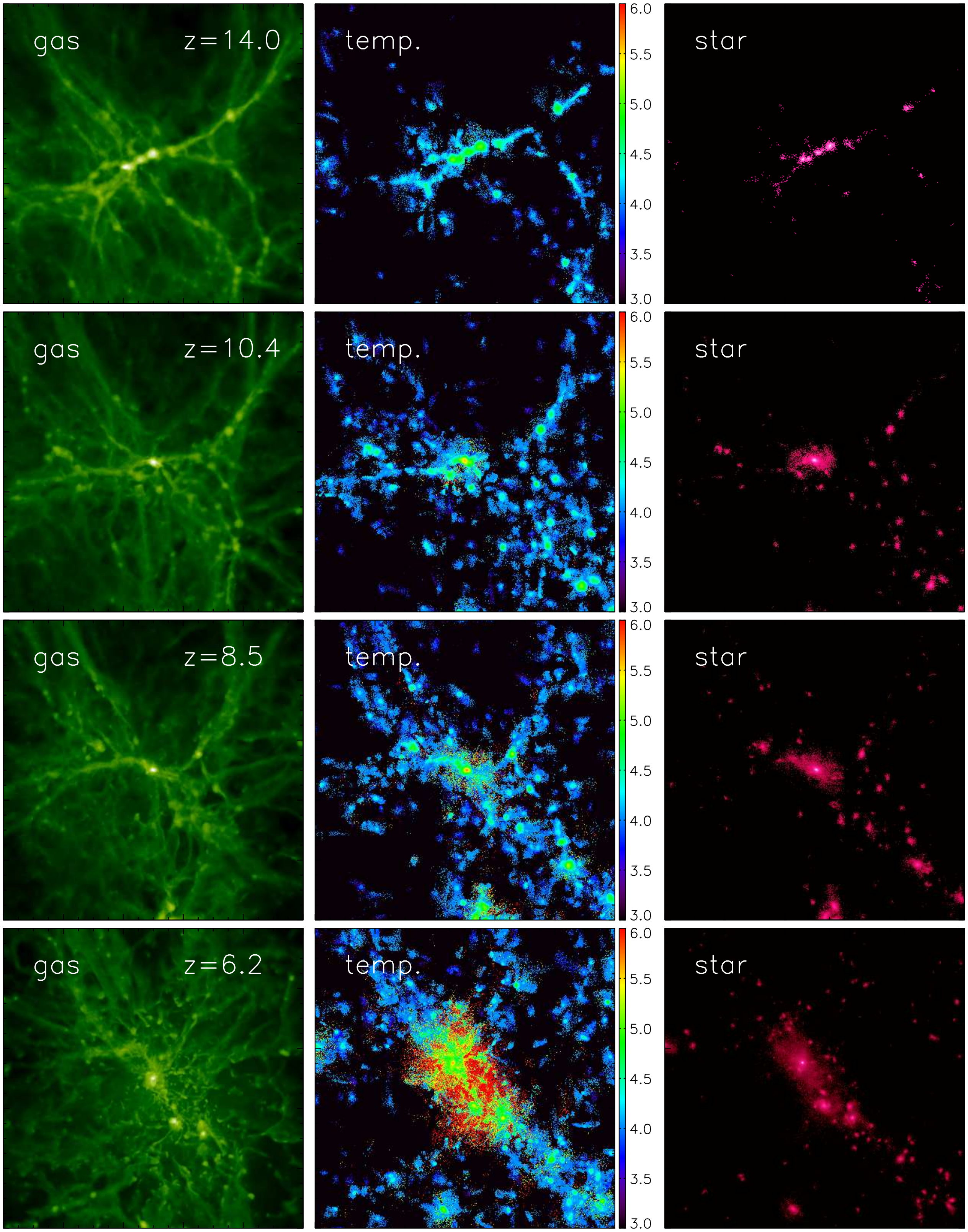

Figure 1. The distribution of gas density (left column), gas temperature (middle column), and stellar density (right column), of the MW galaxy at $z \sim 14, 10.4, 8.5$, and 6.2, respectively. The box size is 1 Mpc in comoving scale. The temperature of the gas is in Kelvin in log scale, as indicated in the color bar.

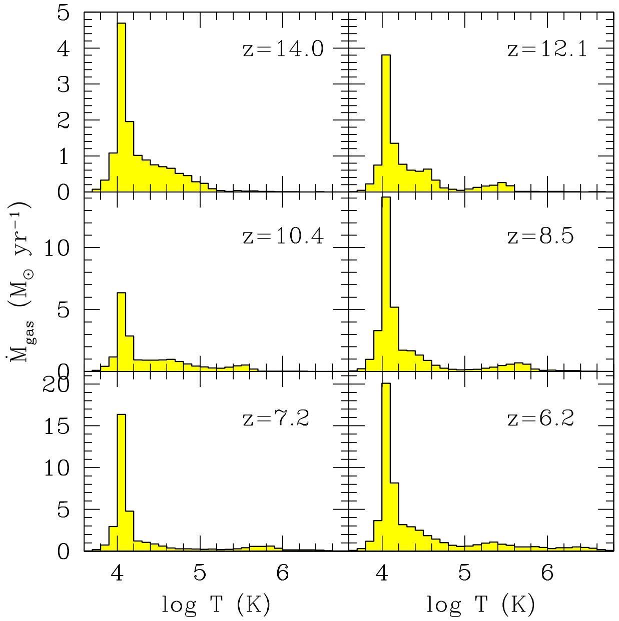

Figure 2. The gas accretion rate by the MW galaxy as a function of gas temperature at different redshift.

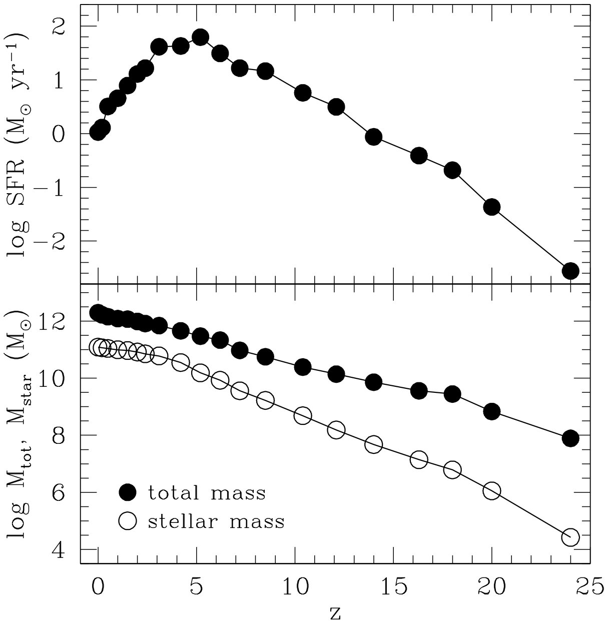

Figure 3. The growth history of the MW galaxy illustrated by the star formation rate (top panel), and by the accumulated mass (bottom panel), in which filled circle represents the total mass, while the open circle represents the stellar mass.

fied as a Lyα emitter (LAE) (e.g., Gronwall et al. 2007). The EW increases with redshift, from ~ 93 Å at $z \sim 6$ to ~ 2300 Å at $z \sim 14.0$. Such trend is in broad agreement with observations that galaxies at higher redshifts appear to have higher EWs than their counterparts at lower redshifts (e.g., Gronwall et al. 2007; Ouchi et al. 2008). This is because the contribution from excitation Lyα cooling becomes large with increasing redshift, as shown in Figure 6 in the next section, which boosts the EW significantly (Yajima et al. 2012a,b).

The currently most distant galaxy detected from Lyα emission line at $z = 8.6$, UDFy-38135539, has a Lyα luminosity of $\sim 5.5 \times 10^{42}\,\mathrm{ergs\,s^{-1}}$ (Lehnert et al. 2010). It is somewhat brighter than our modeled galaxy at the same redshift, indicating that the host galaxy may be more massive than the one in our simulation.

4.3. *Contribution of Excitation Cooling to* Lyα *Emission*

As mentioned in § 3, the Lyα emission is generally produced by the recombination of ionizing photons and the collisional excitation of hydrogen gas. In our cosmological simulation, galaxy evolution is accompanied by cold, filamentary gas streams with temperature $T \sim 10^{4-5}$ K, which penetrate deep inside the dark matter halos (Zhu et al. in prep, Yajima et al. 2012b), a phenomenon also reported by other groups (Katz et al. 2003; Kereš et al. 2005, 2009; Birnboim & Dekel 2003; Dekel & Birnboim 2006; Ocvirk et al. 2008; Brooks et al. 2009; Dekel et al. 2009). Such cold gas can efficiently produce the excitation Lyα cooling photons (Dijkstra & Loeb 2009; Faucher-Giguère et al. 2009; Goerdt et al. 2010). At higher redshift, galaxies experience more merging events and accrete more cold gas efficiently, which results in stronger Lyα emission from excitation cooling, and higher Lyα EWs (Yajima et al. 2012a,b).

As shown in Figure 6, the fraction of excitation cooling Lyα to the total intrinsic Lyα luminosity increases from $\sim 65\%$ at $z \sim 6$ to $\sim 88\%$ at $z \sim 14$. Such extremely high excitation Lyα cooling produces the extremely high Lyα EWs seen in Figure 5.

4.4. *The* Lyα *Line Profile*

The resulting Lyα line profiles of the modeled MW galaxy from $z \sim 14$ to $z \sim 6$ are shown in Figure 7. The frequency of the intrinsic Lyα photon is sampled from a Maxwellian distribution with the gas temperature at the emission location in the rest flame of the gas. All sources show asymmetric profiles with a single peak or weak double peaks. More interestingly, most profiles are shifted to the shorter (bluer) wavelengths. This is a characteristic feature of gas inflow (Zheng & Miralda-Escudé 2002). Indeed, as shown in Figure 8, a significant fraction of the gas shows a large infalling velocity $V_{\rm r} \sim -100$ to ~ -200 km s^{-1}, even though our simulation includes feedback of stellar wind similar to that of Springel et al. (2005). In particular, the gas in the galaxy from $z \sim 14 - 10$ is dominated by inflow motion, which explains the significant blue shift of the profiles in Figure 7 (top panel). At redshift $z \lesssim 8.5$, the gas exhibits outflow as well, and has a larger velocity distribution $-250 \lesssim V_{\rm r} \lesssim 200$ km s^{-1}, which results in an extended profile to both blue and red wings.

We note that the Lyα line profile may be suppressed and changed by the intergalactic medium (IGM) (e.g., Santos 2004; Dijkstra et al. 2007; Zheng et al. 2010; Laursen et al. 2011), because the IGM effectively scatters the Lyα photons at the line center and at shorter wavelengths by the Hubble flow (e.g., Laursen et al. 2011). As a result, the inflow feature in our profiles may disappear and the shape may become an asymmetric single peak with only photons at red wing. However, while

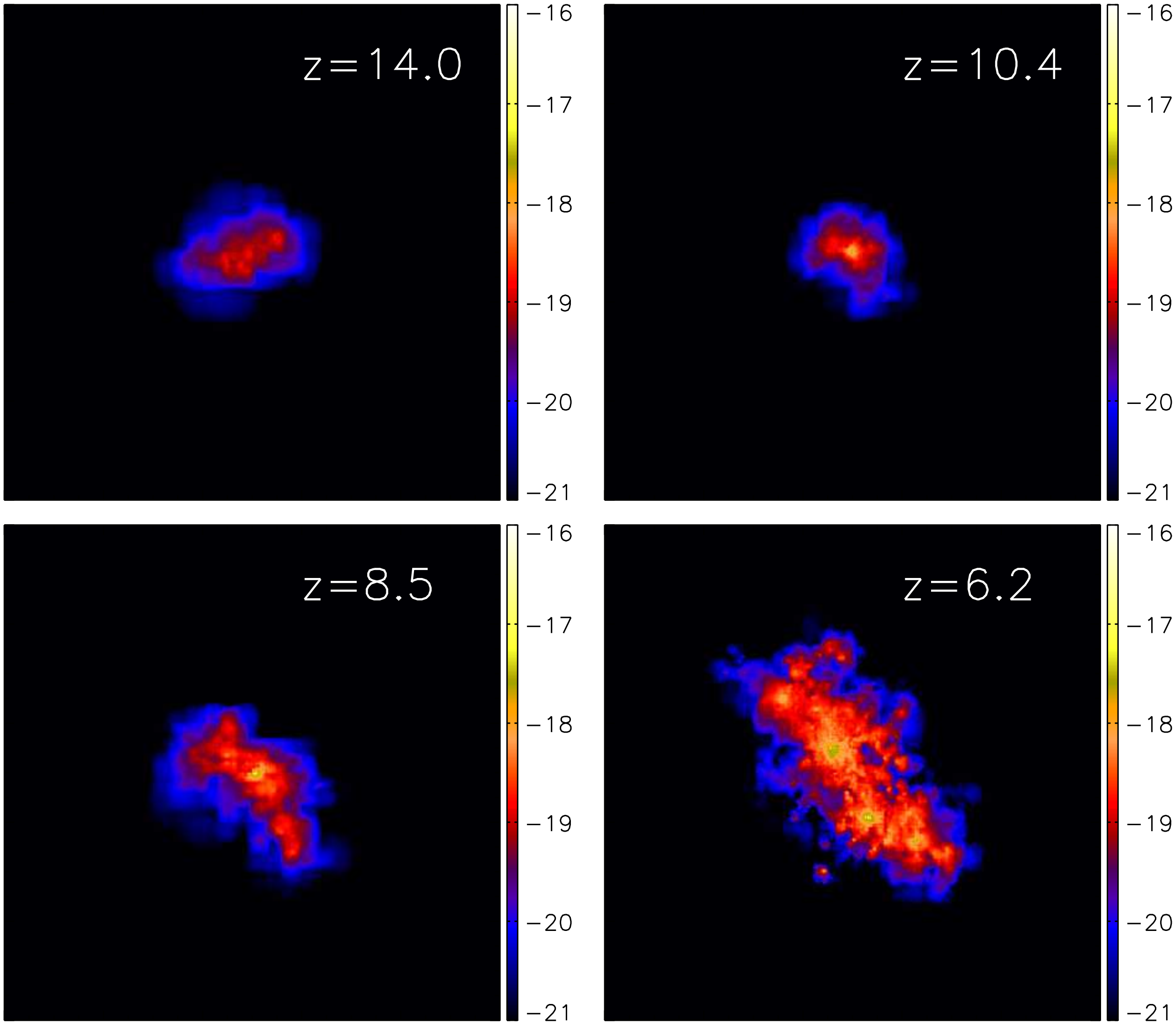

Figure 4. The evolution of the Lyα surface brightness of the MW galaxy with redshift, at $z \sim 14, 10.4, 8.5$, and 6.2, respectively. The box size is 1 Mpc in comoving scale. The color indicates the Lyα surface brightness in log scale in units of ergs s^{-1} cm^{-2} $arcsec^{-2}$.

asymmetric line profiles with an extended red wing are commonly seen in high-redshift LAEs, there appears to be some profiles in the $z \gtrsim 6$ observations that have complex features including double peaks and extended blue wing, similar to what we see here (e.g., Ouchi et al. 2010; Hu et al. 2010; Kashikawa et al. 2011). The observed line of UDFy-38135539, the currently highest redshift galaxy detected at $z = 8.6$, is not resolved and thus has a Gaussian profile (Lehnert et al. 2010). More observations of high-resolution Lyα line profiles of high-redshift LAEs are needed to test our model and verify our predictions.

4.5. *Detectability of Progenitors of Local L^* Galaxies*

The corresponding multi-wavelength SED of the MW galaxy at different redshift are shown in Figure 9. The shape of the SED changes significantly from $z = 14.0$ to $z = 6.2$, as a result of the changes in radiation from stars, absorption of ionizing photons by gas and dust, and re-emission by dust in the infrared. The galaxy shows Lyα line in all cases, and the deep decline of UV continuum at $z \gtrsim 8.5$ is caused by strong absorption of ionizing photons from the dense gas.

A major science goal of the two forthcoming telescopes, ALMA and JWST, is to detect the first galaxies. In order to predict the detectability of the infancy of a local L^* galaxy, we contrast the SEDs with some detection limits of these two facilities in Figure 9. Our calculations show that the flux at 850 μm in the observed frame of the model galaxy ranges from $\sim 7.9 \times 10^{-5}$ mJy at $z = 14.0$ to $\sim 4.7 \times 10^{-2}$ mJy at $z = 6.2$. With an array of 50 antennas and an integration of 10 hours, ALMA may be able to detect such galaxies at $z \lesssim 8.5$ with a 3 σ significance. However, since galaxies do not have a lot of young stars and much dust at $z \gtrsim 10$, observations in continuum by ALMA becomes more difficult, and it would need tens of hours of integration time. In contrast, JWST appears to be more powerful to detect the earliest galaxies as the one we model here, because it can detect the UV continuum in rest frame up to $z \sim 10$. The Lyα emission is strong even at $z \sim 12$, which may be observable by narrow band surveys with similar detection

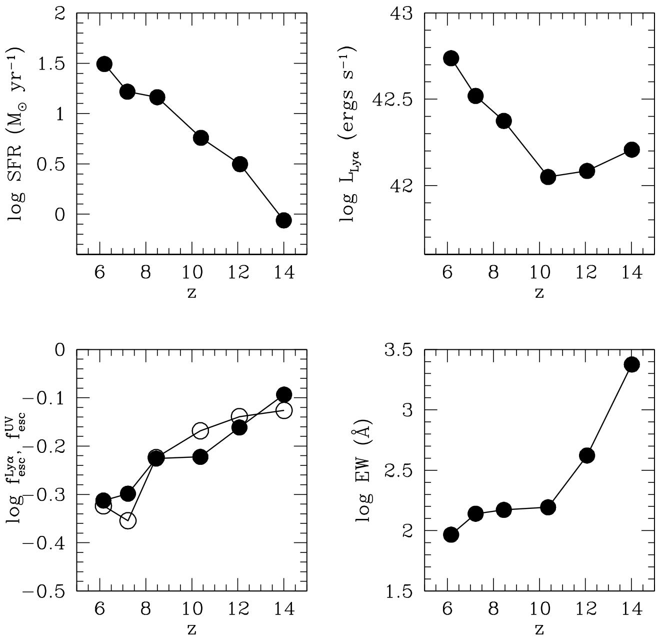

Figure 5. The Lyα properties of the modeled galaxy from $z \sim 14$ to $z \sim 6$, including, in clockwise direction, star formation rate, emergent Lyα luminosity, equivalent width of Lyα line in rest frame, and photon escape fraction of Lyα (filled circles) and UV continuum (1300 - 1600 Å, open circles).

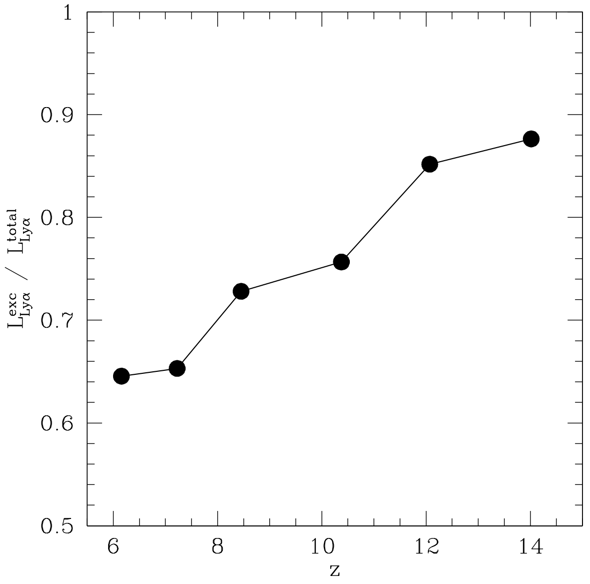

Figure 6. The fraction of excitation cooling Lyα to the total intrinsic Lyα luminosity as a function of redshift from $z \sim 14$ to $z \sim 6$.

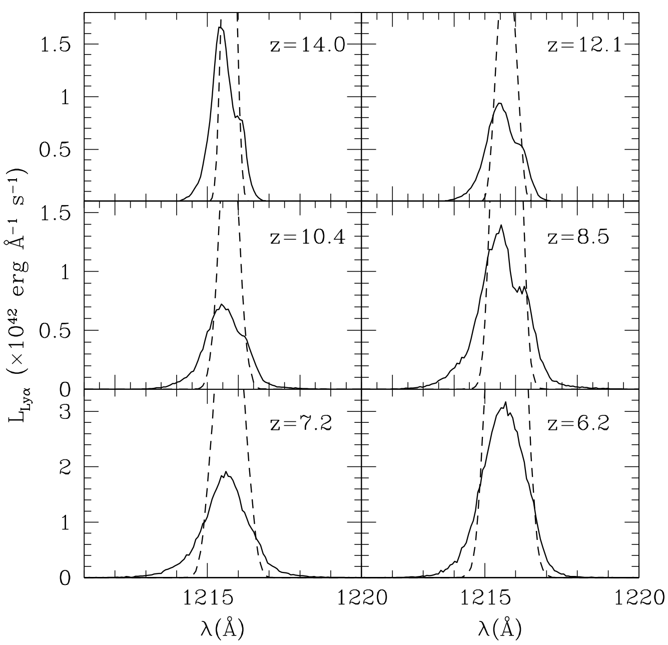

Figure 7. The Lyα line profile of the modeled galaxy at different redshifts. The dotted- and solid lines are the intrinsic and emergent Lyα profile, respectively.

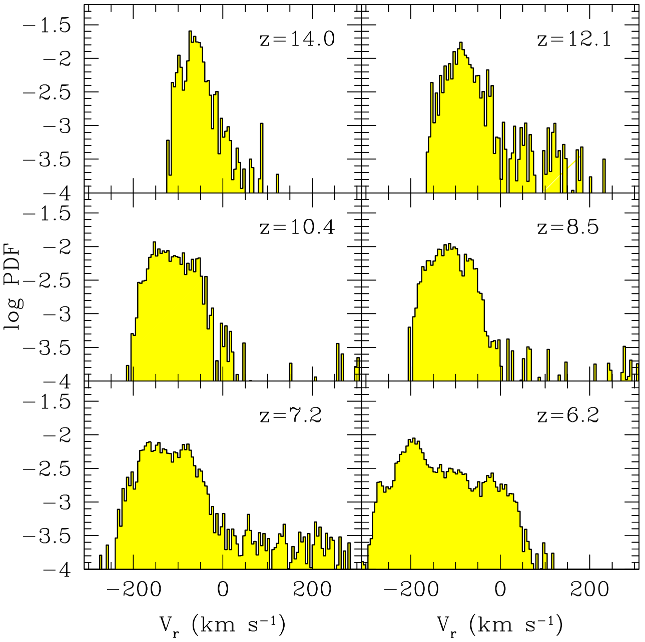

Figure 8. The probability distribution function of the gas mass of the neutral hydrogen in the galaxy as a function of radial velocity. The velocity is estimated from the center of mass of the galaxy in the radial direction.

limit as the JWST. For example, if we use the F164N filter of JWST, the Lyα flux of our galaxy at $z \sim 12$ will be detected at 3 σ with an integration of ~ 20 hours.

We note that in the above estimation, IGM absorption and transmission were not taken into account. The IGM can significantly suppress the Lyα flux, and the transmission highly depends on viewing angle (e.g., Laursen et al. 2011) by inhomogeneous ionization structure in IGM (e.g., Abel et al. 2007; Yoshida et al. 2007; Jeeson-Daniel et al. 2012), which make the detection more difficult. Of course, the galaxies we present here represent progenitor of a local L^* galaxy such as the

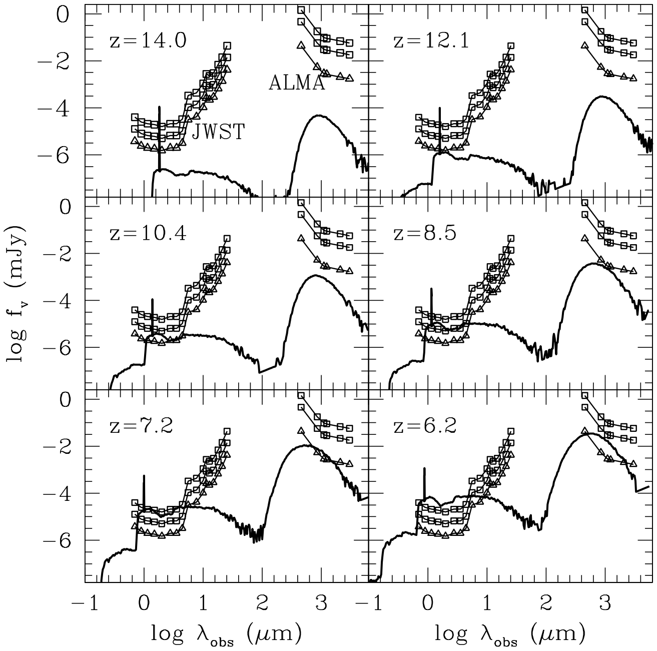

Figure 9. The spectral energy distribution of the MW galaxy at different redshift and its detectability with JWST and ALMA. The open squares indicate the 10 σ detection limits of JWST and ALMA with 16 antennas at an integration time of 1 and 10 hours (from top to bottom), while the open triangles indicate the 3 σ detection limits of JWST and ALMA with 50 antennas.

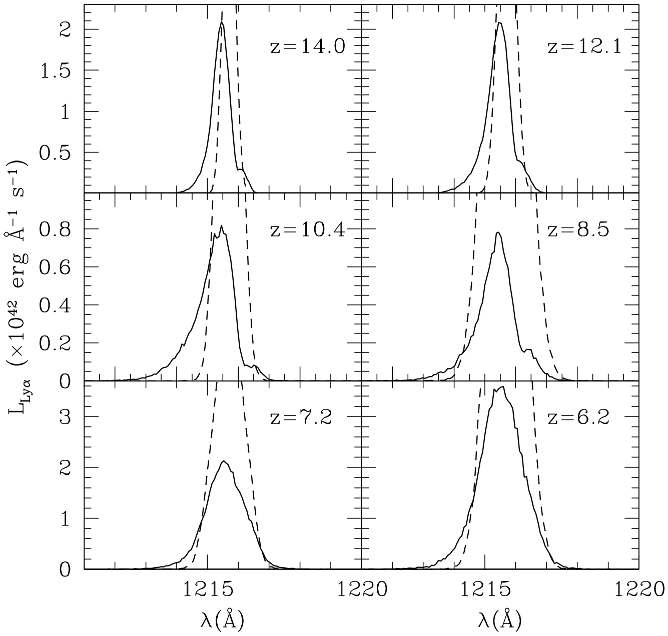

Figure 10. Same as in Figure 7, but here the simulation does not include the wind model from stellar feedback.

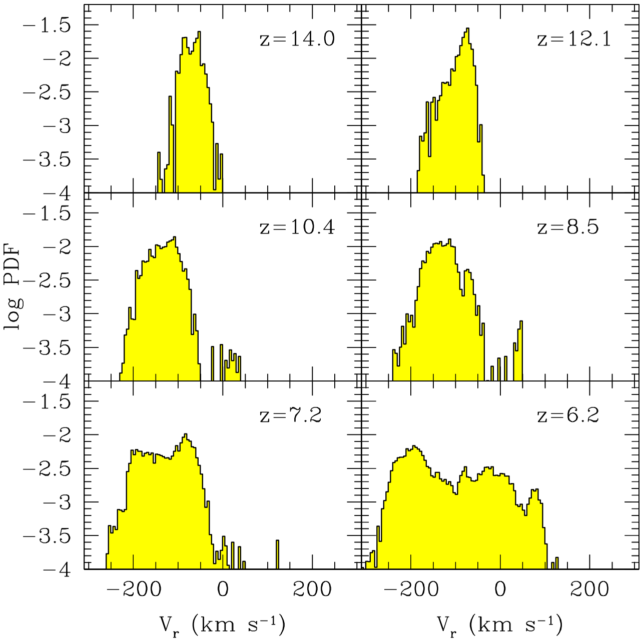

Figure 11. Same as Figure 8, but here the simulation does not include the wind model from stellar feedback. The probability distribution function of the gas mass of the neutral hydrogen in the galaxy as a function of radial velocity. The velocity is estimated from the center of mass of the galaxy in the radial direction.

Milky Way. Galaxies formed in highly overdense regions are likely much more massive (Li et al. 2007), and may be more easily detected by both ALMA and JWST (Li et al, in preparation).

5. DISCUSSIONS

The gas inflow feature is present in our simulation with outflow from stellar feedback. In order to probe the effect of stellar wind on the gas inflow, we also performed the simulation with a pure thermal feedback model, in which the feedback from supernovae is only in thermal energy. In such a model, some fraction of thermal energy can quickly escape as cooling radiation before conversion to kinetic energy. As a result, gas outflow does not occur efficiently.

The resulting Lyα line profiles and the probability distribution function of the neutral gas mass are shown in Figure 10 and Figure 11, respectively. Without a strong outflow, the Lyα line profiles show more pronounced blue wing.

The galaxy in our simulation resides in a low overdensity region and it represents those that would evolve into present-day L^* galaxies such as the MW, so it may not be the very first one formed in the universe. It is believed that the most massive halos in the highly overdense regions collapse first, in which the first stars form (e.g., Abel et al. 2002; Bromm & Larson 2004; Gao et al. 2007; Yoshida et al. 2008). These may also be the formation sites of the very first galaxies, owing to feedback and chemical enrichment from the PopIII stars, as well as abundant gas supply (Li et al. 2007; Bromm et al. 2009).

One of the major limitations of our model is that the cosmological simulation does not have sufficient resolutions to follow the formation and evolution of individual stars. Instead, star formation is modeled using a "subgrid" recipe based on the observed Schmidt-Kennicutt Law (Kennicutt 1998). Gas particles are converted into stars once it is cooled below 10^4 K and the density is above a threshold (Springel & Hernquist 2003). Al-though this treatment is rather simplistic, it nevertheless gives a global star formation history close to what is believed of the MW galaxy.

Another major limitation is that our current RT calculations do not include the propagation and scattering of Lyα and ionizing photons in the IGM. We make the prediction that galaxies with inflow of cold gas would result in asymmetric, blue-shifted Lyα line profiles. However, as discussed earlier, the absorption by IGM may change the the profile to one with extended red wing. We will study this issue in more detail in future work that includes the radiative transfer of Lyα and ionizing photons in the IGM.

6. SUMMARY

In this work, we have investigated the formation of a typical, nearby L^* galaxy such as the MW, and its Lyα properties at the earliest evolutionary stage. We combine a cosmological hydrodynamic simulation, which uses the Aquila initial condition and focuses on a MW-like galaxy, with three-dimensional radiative transfer calculations using the improved ART^2 code, which couples multi-wavelength continuum, Lyα line, and ionization of hydrogen.

We find that the modeled MW galaxy forms from efficient accretion of cold gas early on, which sustains a high star formation rate from $z \sim 14 - 6$. The cold accretion produces strong Lyα emission via collisional excitation, which has a luminosity from $\sim 1.6 \times 10^{42}\,\mathrm{erg\ s^{-1}}$ at $z \sim 14$ to $\sim 5.5 \times 10^{42}\,\mathrm{erg\,s^{-1}}$ at $z \sim 6$. The escape fraction of Lyα photons increases from ~ 0.49 at $z \sim 6$ to ~ 0.81 at $z \sim 14$, due to less dust content at higher redshift. The EWs of the Lyα lines increases with redshift, from ~ 93 Å at $z \sim 6$ to ~ 2300 Å at $z \sim 14$. Such high EWs may be due to significant contribution to Lyα emission by excitation cooling, which dominates at high redshift. The resulting Lyα lines exhibit asymmetric, mostly single-peak profiles shifted to the blue wing, a characteristic feature of inflow.

Furthermore, we demonstrate that progenitors of local L^* galaxies such as the modeled one may be detected at $z \lesssim 8$ by JWST and ALMA with a reasonable integration time. At higher redshift $z \gtrsim 12$, however, only Lyα line may be observable by narrow band surveys with similar detection limit as JWST.

Our results suggest that Lyα line may be used to probe the formation and evolution, and gas properties of distant galaxies. It is perhaps one of the most powerful tools to detect the first generation of galaxies in the coming decade.

We thank Carlos Frenk for kindly providing the Aquila initial conditions to us, and Robin Ciardullo, Mark Dijkstra, Claude-André Faucher-Giguère, Eric Gawiser, Caryl Gronwall, Lars Hernquist, Avi Loeb, Volker Springel and Masayuki Umemura for stimulating discussions and helpful comments. Support from NSF grants AST-0965694 & AST-1009867 (to YL), and AST-0807075 (to TA) is gratefully acknowledged. YL thanks the Institute for Theory and Computation (ITC) at Harvard University where the project was started for warm hospitality. We acknowledge the Research Computing and Cyberinfrastructure unit of Information Technology Services at The Pennsylvania State University for providing computational resources and services that have contributed to the research results reported in this paper (URL: http://rcc.its.psu.edu). The Institute for Gravitation and the Cosmos is supported by the Eberly College of Science and the Office of the Senior Vice President for Research at the Pennsylvania State University.

REFERENCES

Abel, T., Bryan, G. L., & Norman, M. L. 2002, Science, 295, 93
Abel, T., Wise, J. H., & Bryan, G. L. 2007, ApJ, 659, L87
Birnboim, Y. & Dekel, A. 2003, MNRAS, 345, 349
Bouwens, R. J. & Illingworth, G. D. 2006, Nature, 443, 189
Bouwens, R. J., Illingworth, G. D., Labbe, I., et al. 2011, Nature, 469, 504
Bouwens, R. J., Illingworth, G. D., Oesch, P. A., et al. 2010, ApJ, 709, L133
Bouwens, R. J., Thompson, R. I., Illingworth, G. D., et al. 2004, ApJ, 616, L79
Bromm, V. & Larson, R. B. 2004, ARA&A, 42, 79
Bromm, V. & Yoshida, N. 2011, ARA&A, 49, 373
Bromm, V., Yoshida, N., Hernquist, L., & McKee, C. F. 2009, Nature, 459, 49
Brooks, A. M., Governato, F., Quinn, T., Brook, C. B., & Wadsley, J. 2009, ApJ, 694, 396
Bruzual, G. & Charlot, S. 2003, MNRAS, 344, 1000
Davé, R., Hernquist, L., Katz, N., & Weinberg, D. H. 1999, ApJ, 511, 521
Dekel, A. & Birnboim, Y. 2006, MNRAS, 368, 2
Dekel, A., Birnboim, Y., Engel, G., et al. 2009, Nature, 457, 451
Di Matteo, T., Khandai, N., DeGraf, C., et al. 2012, ApJ, 745, L29
Dijkstra, M., Lidz, A., & Wyithe, J. S. B. 2007, MNRAS, 377, 1175
Dijkstra, M. & Loeb, A. 2009, MNRAS, 400, 1109
Faucher-Giguère, C., Kereš, D., Dijkstra, M., Hernquist, L., & Zaldarriaga, M. 2010, ApJ, 725, 633
Faucher-Giguère, C., Lidz, A., Zaldarriaga, M., & Hernquist, L. 2009, ApJ, 703, 1416
Gao, L., Yoshida, N., Abel, T., et al. 2007, MNRAS, 378, 449
Goerdt, T., Dekel, A., Sternberg, A., et al. 2010, MNRAS, 407, 613
Greif, T. H., Glover, S. C. O., Bromm, V., & Klessen, R. S. 2010, ApJ, 716, 510
Gronwall, C., Ciardullo, R., Hickey, T., et al. 2007, ApJ, 667, 79
Haardt, F. & Madau, P. 1996, ApJ, 461, 20
Hernquist, L. & Katz, N. 1989, ApJS, 70, 419
Hu, E. M., Cowie, L. L., Barger, A. J., et al. 2010, ApJ, 725, 394
Hui, L. & Gnedin, N. Y. 1997, MNRAS, 292, 27
Iye, M., Ota, K., Kashikawa, N., et al. 2006, Nature, 443, 186
Jeeson-Daniel, A., Ciardi, B., Maio, U., et al. 2012, MNRAS, 424, 2193
Jeon, M., Pawlik, A. H., Greif, T. H., et al. 2012, ApJ, 754, 34
Kashikawa, N., Shimasaku, K., Matsuda, Y., et al. 2011, ApJ, 734, 119
Katz, N., Keres, D., Dave, R., & Weinberg, D. H. 2003, in Astrophysics and Space Science Library, Vol. 281, The IGM/Galaxy Connection. The Distribution of Baryons at z=0, ed. J. L. Rosenberg & M. E. Putman, 185–+
Katz, N., Weinberg, D. H., Hernquist, L., & Miralda-Escude, J. 1996, ApJ, 457, L57+
Kennicutt, Jr., R. C. 1998, ARA&A, 36, 189
Kereš, D., Katz, N., Fardal, M., Davé, R., & Weinberg, D. H. 2009, MNRAS, 395, 160
Kereš, D., Katz, N., Weinberg, D. H., & Davé, R. 2005, MNRAS, 363, 2
Komatsu, E., Dunkley, J., Nolta, M. R., et al. 2009, ApJS, 180, 330
Latif, M. A., Zaroubi, S., & Spaans, M. 2011, MNRAS, 411, 1659
Laursen, P., Sommer-Larsen, J., & Razoumov, A. O. 2011, ApJ, 728, 52
Lehnert, M. D., Nesvadba, N. P. H., Cuby, J., et al. 2010, Nature, 467, 940
Li, Y., Hernquist, L., Robertson, B., et al. 2007, ApJ, 665, 187

Li, Y., Hopkins, P. F., Hernquist, L., et al. 2008, ApJ, 678, 41
Malhotra, S. & Rhoads, J. E. 2004, ApJ, 617, L5
Ocvirk, P., Pichon, C., & Teyssier, R. 2008, MNRAS, 390, 1326
Ono, Y., Ouchi, M., Mobasher, B., et al. 2012, ApJ, 744, 83
Osterbrock, D. E. & Ferland, G. J. 2006, Astrophysics of gaseous nebulae and active galactic nuclei, ed. Osterbrock, D. E. & Ferland, G. J., Astrophysics of gaseous nebulae and active galactic nuclei
Ouchi, M., Shimasaku, K., Akiyama, M., et al. 2008, ApJS, 176, 301
Ouchi, M., Shimasaku, K., Furusawa, H., et al. 2010, ApJ, 723, 869
Salpeter, E. E. 1955, ApJ, 121, 161
Santos, M. R. 2004, MNRAS, 349, 1137
Scannapieco, C., Wadepuhl, M., Parry, O. H., et al. 2012, MNRAS, 423, 1726
Schmidt, M. 1959, ApJ, 129, 243
Shibuya, T., Kashikawa, N., Ota, K., et al. 2012, ApJ, 752, 114
Springel, V. 2005, MNRAS, 364, 1105
Springel, V., Di Matteo, T., & Hernquist, L. 2005, MNRAS, 361, 776
Springel, V. & Hernquist, L. 2002, MNRAS, 333, 649
—. 2003, MNRAS, 339, 289
Springel, V., Wang, J., Vogelsberger, M., et al. 2008, MNRAS, 391, 1685
Springel, V., Yoshida, N., & White, S. D. M. 2001, New Astronomy, 6, 79
Stark, D. P., Ellis, R. S., & Ouchi, M. 2011, ApJ, 728, L2
Stark, D. P., Ellis, R. S., Richard, J., et al. 2007, ApJ, 663, 10
Vanzella, E., Pentericci, L., Fontana, A., et al. 2011, ApJ, 730, L35
Wadepuhl, M. & Springel, V. 2011, MNRAS, 410, 1975
Wise, J. H. & Abel, T. 2007, ApJ, 665, 899
—. 2008, ApJ, 685, 40
Wise, J. H., Turk, M. J., & Abel, T. 2008, ApJ, 682, 745
Wise, J. H., Turk, M. J., Norman, M. L., & Abel, T. 2012, ApJ, 745, 50
Yajima, H., Li, Y., Zhu, Q., & Abel, T. 2012a, MNRAS, 424, 884
Yajima, H., Li, Y., Zhu, Q., et al. 2012b, ApJ, 754, 118
Yajima, H., Li, Y., Zhu, Q., et al. 2012c, submitted to MNRAS, arXiv: 1209.5842
Yoshida, N., Oh, S. P., Kitayama, T., & Hernquist, L. 2007, ApJ, 663, 687
Yoshida, N., Omukai, K., & Hernquist, L. 2008, Science, 321, 669
Zheng, Z., Cen, R., Trac, H., & Miralda-Escudé, J. 2010, ApJ, 716, 574
Zheng, Z. & Miralda-Escudé, J. 2002, ApJ, 578, 33